EECS 598-07 / NERS 590-06 Fall 2018
Plasma Chemistry and Plasma Surface Interactions

Homework #1: The Basic Global Model for Low Temperature Plasmas

Global models of low temperature plasmas (LTPs) are very effective means of investigating fundamental reaction mechanisms and scaling laws of low and high pressure plasmas. A global model approximates the complex kinetics and chemistry of a plasma using volume averaged quantities. In combustion and chemical engineering, this is called the *well stirred reactor*. Global models are not able to address the details of geometries and spatially dependent phenomena. However, global models are usually able to address much more complex chemistry than can be included in multi-dimensional models. Global models are therefore extremely useful for developing and analyzing reaction mechanisms, and for performing simulations over a large parameter space.

The basic structure of global models for LTPs consists a set of rate equations for densities, temperatures and circuit values (e.g., current, voltage, power), a method of addressing reactions on surfaces, and a method of providing rate coefficients for electron impact processes. These processes are addressed with varying levels of complexity in different global models. The attached paper by Lee et al. discusses a global model for an argon inductively coupled plasma, and is a good example of the general global model for an LTP.

Min-Hyong Lee, Sung-Ho Jang, and Chin-Wook Chung, "On the multistep ionizations in an argon inductively coupled plasma", Physics of Plasmas **13**, 053502 (2006).

1. Read this paper (carefully!) and briefly summarize the findings.

   Based on the results and reaction mechanism discussed in this paper…

2. What is multi-step ionization? In the system modeled by Lee et al in the paper, what are the atomic states involved in multistep ionization?
3. Why is multi-step ionization so effective a source of ionization in rare gas plasmas? (That is, what is it about the atomic structure of rare gas atoms and LTPs sustained in rare gases that enable multi-step ionization?)
4. Why does the energy loss per ion pair (the amount of energy required to create an electron and ion) decrease with increasing power deposition?
5. Why does the electron temperature decrease with increasing pressure?
6. Why does the electron temperature decrease with increasing power deposition?
7. What does the power-transfer efficiency increase with increasing power and then saturate? (You may need to follow-up with References 29 and 30 cited in Lee et al. to learn about the "E-H transition" in inductively coupled plasmas.)

On the multistep ionizations in an argon inductively coupled plasma

Min-Hyong Lee, Sung-Ho Jang, and Chin-Wook Chung[a)]
Department of Electrical and Computer Engineering, Hanyang University, 17 Haengdang-dong, Seongdong-gu, Seoul, 133-791, Republic of Korea

(Received 7 February 2006; accepted 16 March 2006; published online 10 May 2006)

The effect of the multistep ionizations on the plasma parameters in the inductively coupled plasma (ICP) has been investigated by experiments and theory. To obtain electron density and electron temperature precisely at various powers and pressures in the ICP, the electron energy distribution functions (EEDFs) are measured. It is found that at high pressures, the electron temperature from the EEDFs decreases and the electron density increases rapidly with the absorbed power while, at low pressures, the electron temperature is hardly changed and the electron density is almost linearly proportional to the absorbed power. The comparison between the experiment and our model including the multistep ionizations [M. H. Lee and C. W. Chung, Phys. Plasmas **12**, 73501 (2005)] was done and the experiment was in close agreement with the model. This shows that the changes in the electron density and the electron temperature in the ICP are mainly due to the multistep ionizations. © *2006 American Institute of Physics*.

[DOI: 10.1063/1.2193535]

I. INTRODUCTION

Inductively coupled plasma (ICP) is one of the promising plasma sources for the semiconductor industry.[1] Two types of ICP reactors are available. They differ by chamber shape and antenna position. The planar type has a planar coil at the top of the chamber (also called the TCP). The other is the solenoidal type having a solenoidal coil wound around the side of the chamber. It has been reported that the ICP has such advantages of high plasma density ($10^{10}-10^{12}/\mathrm{cm}^3$), a reduction in ion damage, and independently controllable ion energy.[2–6] Also, the ICP has an advantage over other sources in that its hardware does not require external magnetic fields. This makes ICP sources most attractive. Because they are easily scaled up,[7] much research is presently focused on them as the next generation large-area (for wafer) plasma sources.

A global model based on the fluid approximation is well known and commonly used to estimate plasma parameters, such as an electron temperature (T_e), an electron density (n_e), and a plasma potential, etc.[2] The electron temperature is determined by the particle balance between the ionization in the chamber and the loss of the electron-ion pair throughout the chamber wall. On the other hand, the electron density is determined by the power balance between the absorbed power supplied by the rf generator in the plasma and the dissipated power by the particles (electrons and ions) in the plasma. The supplied power is consumed in various ways. Some of it is dissipated to excite or ionize neutral particles by collisions with electrons and some part is lost because electrons and ions carry the kinetic energy to the wall. At a balance point between supplied and dissipated power, the electron density is determined.

In the usual global model, the particle and the power balance equations are not coupled, and therefore, the electron temperature, which is a function of the pressure and the effective plasma size, is independent of the electron density. However, experimental results show that the electron temperature decreases when the rf power (electron density) increases.[8] In the power balance equation, the decrease of the electron temperature hardly changes the loss of an electron and an ion, and reduces only the ionization. Therefore, for the conservation of particles, additional ionization process such as multistep ionizations should be needed.

There have been a number of studies about the metastable state and multistep ionizations in the dc and rf dischargers.[9–14] The spatial density profile of metastable atoms was simulated[9] and two and three-dimensional distribution of metastable atoms was experimentally measured[10–12] at various powers and pressures by spectroscopy. A transition of sustaining mechanism of ICP from direct ionization to multistep ionization with an increase in the pressure and input power is also reported.[13] The metastable density does not simply increase with the absorbed power due to the electron induced quenching.[11] The multistep ionization lowers the bulk electric field and the electron energy, and increases the plasma density at high pressure.[9,14] In the ICP, the plasma is sustained with lower energy electrons, and therefore, the multistep ionizations are of importance.[14]

We recently developed a modified particle and power balance equation including multistep ionizations.[15,16] In this study, we measured the electron energy probability functions (EEPFs) at various pressures and absorbed powers in an inductively coupled plasma and we obtained the electron temperature and the electron density from them. By comparing the experimental results with our modified model, we experimentally verify that our modified global model represents well the effects of multistep ionizations on the plasma parameters in an inductively coupled plasma.

[a)]Author to whom correspondence should be addressed. Electronic mail: joykang@hanyang.ac.kr

II. EXPERIMENTAL APPARATUS AND SETUP

Figure 1 shows a schematic of an experimental setup. Measurements are done in a cylindrical inductively discharge reactor whose radius (R) and length (L) are 23 cm and 16 cm, respectively. A one turn cooper coil antenna with a radius of 15 cm is placed on the quartz plate and 13.56 MHz power up to 1200 W can be delivered to the antenna through an alternative matching network.

A rf compensated single Langmuir probe made of 10 mm long and 0.1 mm in diameter tungsten wire is placed at the center of the reactor. The probe system consists of a floating loop reference probe and 13.56 MHz resonance filter which reduces the rf distortion of probe characteristics and a small measurement probe.[17,18] The second derivative of the probe current with respective to the probe potential (I_e''), which is proportional to the electron energy distribution function $f(\epsilon)$, is obtained by numerical differentiating and smoothing.[19] The measured second derivative I_e'' is related to the electron energy distribution function $g(\epsilon)=\epsilon^{1/2}f(\epsilon)$ as follows:[2]

$$g(\epsilon) = \frac{2m}{e^2 A}\left(\frac{2\epsilon}{m}\right)^{1/2} I_e''(\epsilon), \tag{1}$$

where ϵ, e, m, and A are the electron energy, charge, mass, and probe area, respectively. Electron density n_e, plasma potential V_p, and electron temperature T_e can be calculated from the EEPF $f(\epsilon)$.[2]

A Pearson transformer is placed and connected to a digital oscilloscope to measure the current flowing through the antenna as shown in Fig. 1. Because the antenna and the matching system have a real resistance, the supplied rf power is consumed not only in the plasma chamber but at the antenna and the matching system as a Joule heating. Therefore, to measure the absorbed power that consumed by the plasma only, we should measure the circuit resistance (resistance of the antenna and the matching system). The current flowing through the circuit is given as $I=(P_{\mathrm{rf}}/R_{\mathrm{circuit}})^{1/2}$ when the plasma is turned off. Here P_{rf} is a supplied rf power and R_{circuit} is a circuit resistance. By measuring currents with respect to rf powers, the circuit resistance of our system is found to be 0.48 Ω.

When the plasma is turned on, the absorbed power that is consumed by the plasma only is given by $P_{\mathrm{abs}}=P_{\mathrm{rf}}-I^2R_{\mathrm{circuit}}$. By defining the power transfer efficiency α as

$$\alpha \equiv \frac{P_{\mathrm{abs}}}{P_{\mathrm{rf}}} = 1 - \frac{I^2 R_{\mathrm{circuit}}}{P_{\mathrm{rf}}}, \tag{2}$$

the absorbed power can be obtained as the following:

$$P_{\mathrm{abs}} = \alpha P_{\mathrm{rf}}. \tag{3}$$

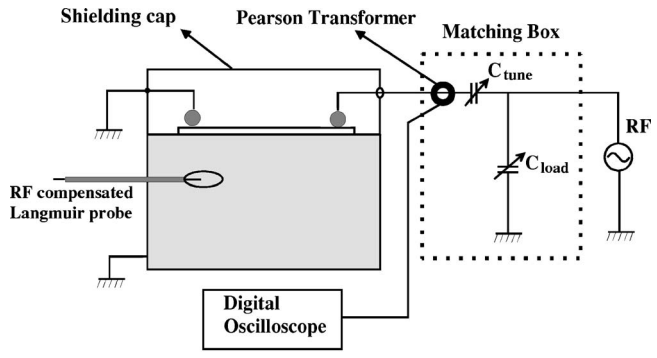

FIG. 1. A schematic of an experimental arrangement.

III. GLOBAL MODEL INCLUDING THE MULTISTEP IONIZATIONS

A. Particle balance equation

A schematic diagram of an argon atom energy levels is shown in Fig. 2. $^1P_1$ and $^3P_1$ states are resonance states and are represented as the $4s_r$ state. $^3P_0$ and $^3P_2$ states are metastable states and are represented as the $4s_m$ state. The $4p$ excited state has 10 energy levels in the range of 12.9–13.5 eV. Because the energy levels of $4s_r$ and $4s_m$ states are very close, we consider them to have the same energy level. $4s_r$, $4s_m$, and $4p$ state atom densities in this paper represent total densities of all the energy levels belonging to the $4s_r$, $4s_m$, and $4p$ manifold, respectively.[20,21] All reactions and corresponding rate constants included in our calculation are listed in Table I.[2,22–26] In Table I, K_{el} represents an elastic collision rate constant, K_{gi}, K_{mi}, K_{ri}, and K_{pi} represent ionization rate constants from ground state, $4s$ metastable states, $4s$ resonance states, and $4p$ excited states, respectively, and K_{gm}, K_{gr}, K_{gp}, K_{mp}, and K_{rp} represent excitation rate constants by electron collision. K_{mg}, K_{rg}, K_{pg}, K_{pm}, and K_{pr} in Table I represent the rate constants of superelastic collision that a higher energy state atom loses its energy and makes a transition to a lower energy state by collision with an electron. It should be notified that rate constants in Table I were obtained with an assumption of Maxwellian distribu-

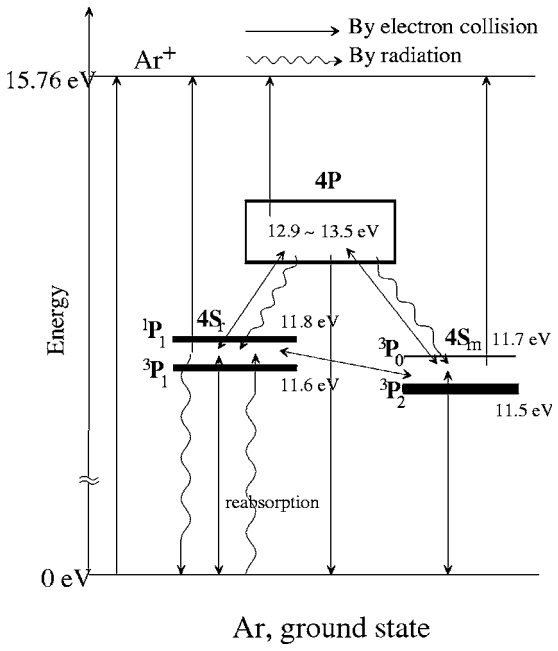

FIG. 2. A schematic diagram of energy levels and transitions of an argon atom.

TABLE I. Reactions and corresponding rate constants of argon used in calculations. Subscripts r and m denote resonance and metastable levels of the $4s$ excited state and subscript p denotes the $4p$ excited state. Units of K are $m^3\ s^{-1}$ and A are s^{-1}.

Reaction	Rate Constant	Ref.
$Ar+e$ elastic collision	$K_{el}=2.3\times10^{-14}T_e^{1.61}\exp(0.06(\ln T_e)^2-0.12(\ln T_e)^3)$	Ref. 2, p. 81
$Ar+e\rightarrow Ar^+ +2e$	$K_{gi}=2.3\times10^{-14}T_e^{0.68}\exp(-15.76/T_e)$	Ref. 22
$Ar_m+e\rightarrow Ar^+ +2e$	$K_{mi}=6.8\times10^{-15}T_e^{0.67}\exp(-4.2/T_e)$	Ref. 2, p. 81
$Ar_r+e\rightarrow Ar^+ +2e$	$K_{ri}=6.8\times10^{-15}T_e^{0.67}\exp(-4.2/T_e)$	Ref. 2, p. 81
$Ar_p+e\rightarrow Ar^+ +2e$	$K_{pi}=1.8\times10^{-13}T_e^{0.61}\exp(-2.61/T_e)$	Ref. 2, p. 81
$Ar+e\rightarrow Ar_m+e$	$K_{gm}=2.5\times10^{-15}T_e^{0.74}\exp(-11.56/T_e)$	Ref. 2, p. 81
$Ar+e\rightarrow Ar_r+e$	$K_{gr}=2.5\times10^{-15}T_e^{0.74}\exp(-11.56/T_e)$	Ref. 2, p. 81
$Ar+e\rightarrow Ar_p+e$	$K_{gp}=1.4\times10^{-14}T_e^{0.71}\exp(-13.2/Te)$	Ref. 2, p. 81
$Ar_m+e\rightarrow Ar+e$	$K_{mg}=4.3\times10^{-16}T_e^{0.74}$	Ref. 2, p. 18
$Ar_r+e\rightarrow Ar+e$	$K_{rg}=4.3\times10^{-16}T_e^{0.74}$	Ref. 2, p. 81
$Ar_p+e\rightarrow Ar+e$	$K_{pg}=3.9\times10^{-16}T_e^{0.71}$	Ref. 2, p. 81
$Ar_m+e\rightarrow Ar_r+e$	$K_{mr}=2.0\times10^{-13}$	Ref. 2, p. 81
$Ar_m+e\rightarrow Ar_p+e$	$K_{mp}=8.9\times10^{-13}T_e^{0.51}\exp(-1.59/T_e)$	Ref. 23
$Ar_r+e\rightarrow Ar_p+e$	$K_{rp}=8.9\times10^{-13}T_e^{0.51}\exp(-1.59/T_e)$	Ref. 23
$Ar_r+e\rightarrow Ar_m+e$	$K_{rm}=3.0\times10^{-13}$	Ref. 24
$Ar_p+e\rightarrow Ar_m+e$	$K_{pm}=1.5\times10^{-13}T_e^{0.51}$	Ref. 22
$Ar_p+e\rightarrow Ar_r+e$	$K_{pr}=1.5\times10^{-13}T_e^{0.51}$	Ref. 22
$Ar_r\rightarrow Ar+h\nu$	$A_{pm,\mathrm{eff}}$, Eq. (9)	Ref. 22
$Ar_p\rightarrow Ar_m+h\nu$	$A_{pm,\mathrm{eff}}=3\times10^7$	Ref. 25
$Ar_p\rightarrow Ar_r+h\nu$	$A_{pr,\mathrm{eff}}=3\times10^7$	Ref. 25
$D_{\mathrm{eff}}n_g$	1.0×10^{20} $(m^{-1}\ s^{-1})$	Ref. 26

tion of electrons, and therefore, the calculated results in our paper are also good when the system is in the Maxwellian distribution.

The particle balance equations of each excited state are written as[15]

$$\frac{dn_m}{dt}=K_{gm}n_gn_e+K_{rm}n_rn_e+(K_{pm}n_e+A_{pm,\mathrm{eff}})n_p-\left\{(K_{mr}+K_{mp}+K_{mg}+K_{mi})n_e+\frac{D_{\mathrm{eff}}}{\Lambda^2}\right\}n_m=0, \tag{4}$$

$$\frac{dn_r}{dt}=K_{gr}n_gn_e+(K_{pr}n_e+A_{pr,\mathrm{eff}})n_p+K_{mr}n_mn_e-\left\{(K_{rp}+K_{rm}+K_{rg}+K_{ri})n_e+A_{r,\mathrm{eff}}+\frac{D_{\mathrm{eff}}}{\Lambda^2}\right\}n_r=0, \tag{5}$$

$$\frac{dn_p}{dt}=K_{gp}n_gn_e+K_{mp}n_mn_e+K_{rp}n_rn_e-\left\{(K_{pm}+K_{pr}+K_{pg}+K_{pi})n_e+A_{pm,\mathrm{eff}}+A_{pr,\mathrm{eff}}+\frac{D_{\mathrm{eff}}}{\Lambda^2}\right\}n_m=0, \tag{6}$$

where n_g, n_m, n_r, n_p, and n_e are atom densities of ground state, $4s_m$, $4s_r$, $4p$ state and electron density, respectively, and $D_{\mathrm{eff}}n_i/\Lambda^2$ is a diffusive loss rate of atoms to the chamber walls. The detailed model of the power balance equation including the multistep ionization follows our previous work.[15] The balance equation between the electron-ion production and loss including the multistep ionizations is

$$\sum_i VK_{iz,i}n_in_e=V(K_{gi}n_g+K_{mi}n_m+K_{ri}n_r+K_{pi}n_p)n_e=n_eu_B(A_lh_l+A_rh_r), \tag{7}$$

where $V=\pi R^2L$ is a plasma volume, u_B is Bohm velocity, $A_l=2\pi R^2$ and $A_r=2\pi RL$ are sheath areas of axial and radial directions, respectively, and h_l and h_r are expressed as the following when the mean free path for neutral-ion collisions is λ_i,[27]

$$h_l\approx0.86\left(3+\frac{L}{2\lambda_i}\right)^{-1/2},$$

$$h_r\approx0.80\left(4+\frac{R}{2\lambda_i}\right)^{-1/2}.$$

Some parts of the emitted photons from the excited resonance state will be reabsorbed by ground state atoms. This brings a decrease in the decay rate and the effective decay rate should be considered. We follow the model of Asida *et al.*[22] for the effective decay rate. They assume that an emission that occurred within mean free path from the chamber wall can escape without reabsorption. Therefore, the effective decay rate (A_{eff}) is given as the following when the normal decay rate is A:

$$A_{\mathrm{eff}}=A\frac{V_{\mathrm{escape}}}{V_{\mathrm{total}}}=2A\left(\frac{1}{R}+\frac{1}{L}\right)\frac{1}{n_g\sigma}, \tag{8}$$

where R and L are the chamber radius and the length, and σ is an optical absorption cross section. However, because the inner wall of our chamber is made by stainless steel, the light

reaching the wall will be reflected into the plasma and reabsorbed. The emission can escape through only small glass windows and a quartz plate whose area is about 10% of the total surface area of the chamber. With this correction, the effective decay rate from the $4s_r$ state to the ground state is calculated in our chamber as the following:

$$A_{rg,\mathrm{eff}} = \frac{8 \times 10^6}{p}, \tag{9}$$

where p is pressure in mTorr.

B. Power balance equation

The supplied energy to the plasma is lost by collisional and kinetic energy loss.[2] The kinetic energy loss (P_k) becomes

$$P_k = n_e u_B(\varepsilon_i + 2T_e)(A_l h_l + A_r h_r) = n_e u_B\left(eV_s + \frac{T_e}{2} + 2T_e\right) \times (A_l h_l + A_r h_r), \tag{10}$$

and the collisional energy loss (P_c) becomes

$$P_c = n_e u_B \varepsilon_c (A_l h_l + A_r h_r). \tag{11}$$

Here, ε_i and ε_c are the mean kinetic energy lost per ion lost and the collisional energy loss per electron-ion created, respectively. By considering multistep ionizations from $4s_r$, $4s_m$, and $4p$ states, ε_c is given as follows:[15,16]

$$\begin{aligned}(K_{gi}n_g + K_{mi}n_m + K_{ri}n_r + K_{pi}n_p)n_e\varepsilon_c &= \Big[(K_{gm}\varepsilon_{gm} + K_{gr}\varepsilon_{gr} + K_{gp}\varepsilon_{gp})n_g n_e \\ &+ \left(K_{gi}n_g\varepsilon_{gi} + K_{mi}n_m\varepsilon_{mi} + K_{ri}n_r\varepsilon_{ri} + K_{pi}n_p\varepsilon_{pi} + K_{\mathrm{el}}\frac{3m}{M}T_e\right)n_e + (K_{mp}\varepsilon_{mp} - K_{mg}\varepsilon_{gm})n_m n_e + (K_{rp}\varepsilon_{rp} \\ &- K_{rg}\varepsilon_{gr})n_r n_e - (K_{pg}\varepsilon_{gp} + K_{pm}\varepsilon_{mp} + K_{pr}\varepsilon_{rp})n_p n_e\Big].\end{aligned} \tag{12}$$

Here, M and m are the neutral mass and electron mass, and ε_{jk} represents the ionization or excitation energy to transit from the j state to the k state. With this ε_c, the total power balance equation including multistep ionizations can be expressed as

$$P_{\mathrm{abs}} = P_k + P_c = n_e u_B\left(\varepsilon_c + eV_s + \frac{5T_e}{2}\right)(A_l h_l + A_r h_r), \tag{13}$$

and the electron density is given from Eq. (13) as the following:

$$n_e = \frac{P_{\mathrm{abs}}}{A_{\mathrm{eff}} u_B(\varepsilon_c + eV_s + 5T_e/2)}. \tag{14}$$

Here, $A_{\mathrm{eff}} = A_l h_l + A_r h_r$ is the total sheath area.

Equations (7) and (13) are particle and power balance equations including multistep ionizations, and by solving these equations in a self-consistent manner, we can find out the effects of the multistep ionizations on the electron temperature and the electron density.

IV. EXPERIMENTAL RESULTS AND DISCUSSION

Figure 3(a) shows the measured power transfer efficiencies α at various argon pressures as a function of input rf powers. This shows that the power transfer efficiency is almost proportional to the rf power in the low rf power region ($\alpha \ll 1$). This is consistent with the previous report.[28] Because the circuit resistance is hardly changed with rf power, the increase in the efficiency indicates the increase in the resistance of the plasma. It is notable that the efficiency at 3 mTorr argon pressure increases abruptly at the rf power of about 70 W. The abrupt increase in the efficiency leads to a jump in the absorbed power, and therefore, a jump in the

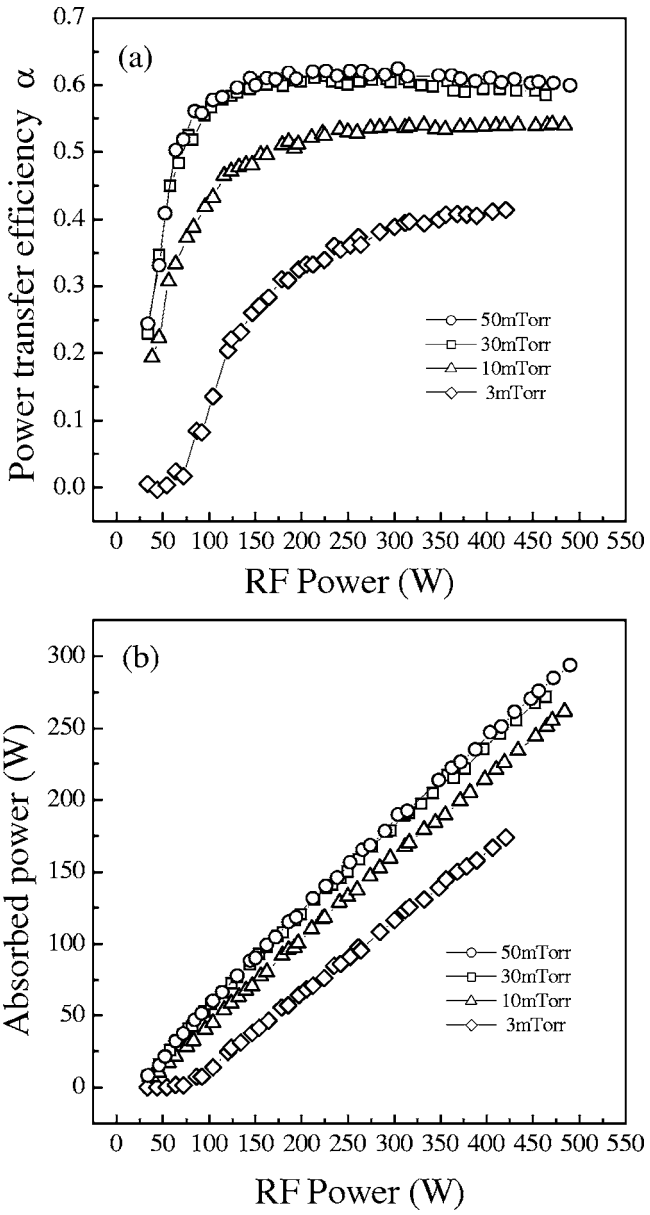

FIG. 3. Experimental points of (a) the power transfer efficiency and (b) absorbed power that is consumed by plasma only as a function of rf power at various pressures.

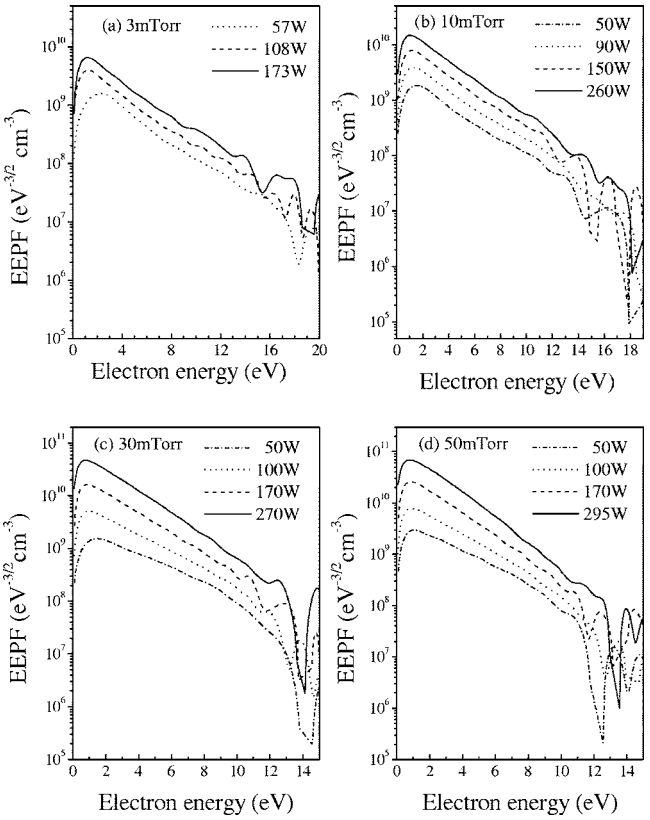

FIG. 4. The measured EEPFs at various absorbed powers in (a) 3 mTorr, (b) 10 mTorr, (c) 30 mTorr, and (d) 50 mTorr.

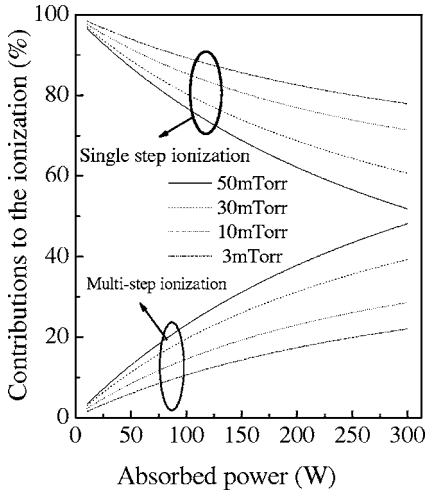

FIG. 5. Contributions of single step and multistep ionizations to the total ionization at various pressures and absorbed powers.

electron density, which is known as a density jump at the $E-H$ transition.[29,30] The absorbed power supplied to the plasma is given by $P_{abs}=\alpha P_{rf}$, and shown in Fig. 3(b).

The measured EEPFs at the various absorbed powers and pressures are presented in Fig. 4. The minus inverse of a slope of the EEPF is proportional to the electron temperature.[2] Figure 4(a) shows that, at low pressure (3 mTorr), low and high energy electrons have different temperatures, i.e., electron distribution is in a bi-Maxwellian distribution. This is mainly caused by two factors. One is the Ramsauer effect and the other is a trapping of low energy electrons in an ambipolar potential barrier.[31,32] At high pressure and low power, the EEPFs are Druyvesteyn-type, which is also caused by the Ramsauer effect. All the EEPFs are evolved to the single Maxwellian distribution with increasing absorbed power (electron density) due to the increase in electron-electron collisions. Note that at higher pressure the slopes of the EEPFs become steeper with the absorbed power and this indicates the decrease in the electron temperature [Figs. 4(c) and 4(d)]. On the other hand, the slopes are hardly changed at low pressure [Fig. 4(a)]. From the point of view of the particle balance, the decrease of the electron temperature indicates that the electron generation becomes effective. This is mainly due to the multistep ionization effect.[15,16] Multistep ionizations increase the ionization, although the loss of the electron-ion pair, which generally depends on the size of the sheath area, does not change. Therefore, to balance between ionization and loss of the electron and the ion, the ionization rate of the pair should be lower and this leads to a decrease in the electron temperature.

Figure 5 shows the contributions of single step and multistep ionizations to total ionizations as a function of absorbed power. As suggested by Sato *et al.*,[13] the multistep ionization effect becomes prominent with increasing pressure. There are two factors for this: electron density and reabsorption of a radiated light. In the multistep process, the neutral species should collide two or more times with electrons, while, in the single step process, the neutral particle collides only one time to be an ion. Because the electron density is proportional to the pressure at the same absorbed power, at high pressure, where the probability to collide with an electron becomes larger, multistep ionizations become more dominant than those at low pressure. The other factor related to the pressure dependence of the contribution is the reabsorption effect of radiated lights. As can be seen in Eq. (9), the effective decay rate becomes smaller as the pressure increases. The probability of the reabsorption of the emitted light is certainly proportional to the density of the ground state atom which is also proportional to the pressure. Therefore, the increase in the pressure induces the increase in the atomic density of excited states, and this makes the effect of the multistep ionizations become significant at high pressure. The EEPFs in Fig. 4 show this clearly. The slopes of the EEPFs of high pressures [Figs. 4(c) and 4(d)] are changed rapidly with absorbed power while those at low pressures are hardly changed [Figs. 4(a) and 4(b)].

The electron temperatures from the EEPFs at 10 mTorr and 30 mTorr versus the absorbed power are shown in Fig. 6. Experimental and theoretical results show well the decrease in the electron temperature with increasing the absorbed power. The results also show that the electron temperature at 30 mTorr decreases more steeply than at 10 mTorr. This is in agreement with the pressure dependence of the multistep contribution as shown in Fig. 5. As can be seen in Fig. 6, measured ones show more rapid decrease in the electron temperature compared with the calculations. This may be caused from an underestimation of multistep

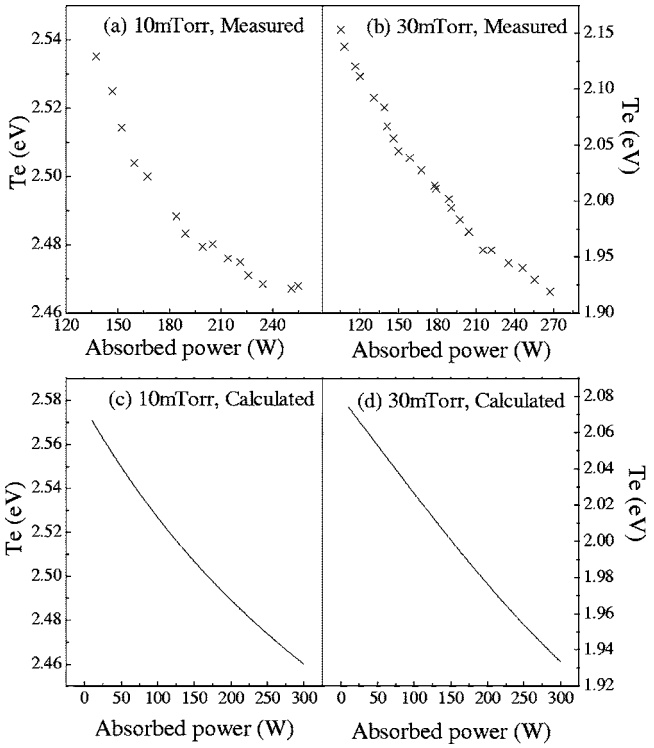

FIG. 6. Measured and calculated electron temperatures at 10 mTorr (a) and (c) and 30 mTorr (b) and (d).

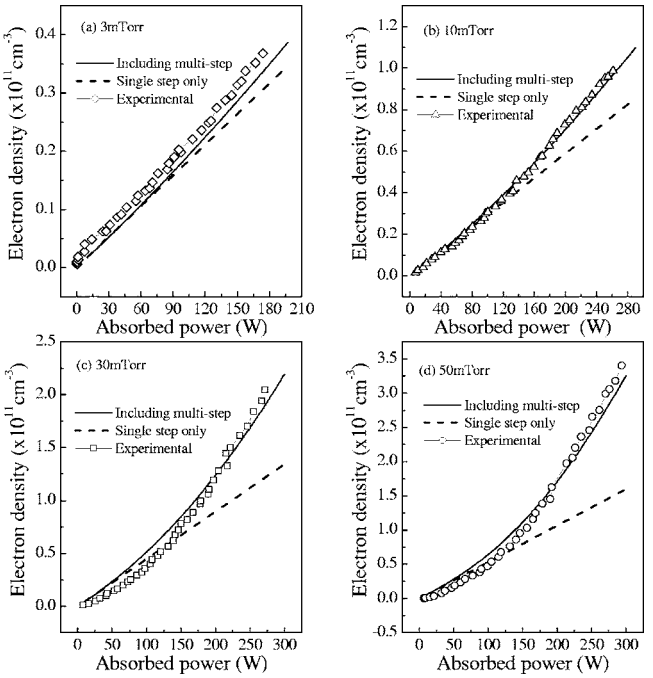

FIG. 8. Electron densities measured and calculated with (solid lines) and without multistep ionizations (dotted lines) at the pressures of (a) 3 mTorr, (b) 10 mTorr, (c) 30 mTorr, and (d) 50 mTorr.

ionizations in our calculations. We consider only $4s_r$, $4s_m$, and $4p$ excited states, while so many excited states such as $3d$, $4d$, $5s$, and $5d$ states exist in an argon atom. Therefore, the multistep effect in fact may be larger than our consideration and this makes a slight difference between the experiment and the calculation.

Figure 7 shows the change in the collisional energy loss per electron-ion pair created (ε_c) against the absorbed power. Electron temperature and average ionization energy are two factors that ε_c by the multistep ionizations changes. As presented in Fig. 6, the multistep effect decreases the electron temperature. Although the decrease in the electron temperature decreases the kinetic energy loss as shown in Eq. (10), this acts to increase the electron density, the collisional energy loss, and thus, ε_c in Eq. (11) is also changed with the electron temperature. In Eq. (12), ε_c is a function of ionization and excitation rate constants which are also functions of the electron temperature. The decrease in the electron temperature brings a decrease in rate constants and, as a result, increases in the ε_c.[2] Therefore, the multistep effect can decrease the electron density as can be seen in Eq. (13) at the point of only the electron temperature. However, multistep ionizations lower the mean energy needed to create one electron-ion pair. The atom in the excited state can jump into the ion with small energy compared to the ground state atom, and therefore, total energy loss of an electron to create an electron-ion pair will decrease as the multistep effect increases. This leads to a severe drop of ε_c and thus an increase in the electron density. As a result, multistep ionization affects ε_c in two opposite ways; the decrease of the electron temperature may cause an increase in ε_c, and the lowering of the mean energy to create an electron-ion pair decrease in ε_c. However, the change of electron temperature due to the multistep effect is small, and multistep ionizations lower ε_c as shown in Fig. 7.

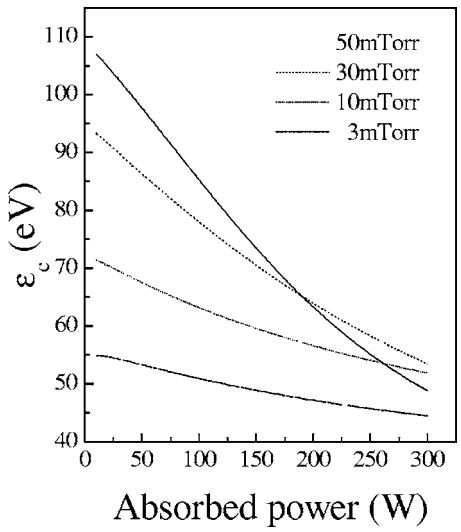

FIG. 7. Changes in the collisional energy loss per electron-ion pair created (ε_c) against the absorbed power at various pressures.

In Fig. 8, we present the change of the electron density as a function of the absorbed power at various argon pressures. Solid and dotted lines represent calculated electron densities including multistep ionizations and single step ionization only, respectively. Scattered dots are measured ones. Electron densities with multistep ionizations are higher than those of the single step only. At 50 mTorr pressure and 300 W absorbed power, the solid line (including multistep ionizations) shows more than two times higher electron den-

sity than the dotted line (single step ionization only). This is due to the additional ionization processes of multistep ionizations. The difference between solid and dotted lines becomes larger as the pressure increases because multistep ionizations become apparent with the pressure. Experimental results agree well with solid lines in a wide pressure range as shown in Fig. 8.

Dotted lines are proportional to the absorbed power in all pressure ranges as expected from the standard global model.[2] However, solid lines are no more linear and increase very rapidly with the absorbed power. The nonlinearity of the increase in the electron density is due to the change of ε_c. ε_c becomes abruptly low with increasing the absorbed power and from Eq. (14), this makes the slopes of the increase in the electron density steeper. Because the lowering of ε_c is proportional to the pressure as shown in Fig. 7, the deviation from a linear becomes larger as the pressure increases.

V. CONCLUSION

In this study, we investigate the effects of multistep ionizations and compare the effects with experimental results in an argon ICP. The EEPFs at various pressures show that the electron temperature decreases with the absorbed power. The decrease in temperature is small at low pressure and becomes larger with higher pressure. The measured electron density with power is no more linear to the absorbed power, which is contrary to the standard global model. The nonlinearity increases with the pressure. All of these can be explained by multistep ionization effects. Because multistep ionizations increase the ionization without changing the loss, the electron temperature should decrease to meet the particle balance. Multistep ionizations also lower the mean energy required to create an electron-ion pair. Because ε_c decreases with the absorbed power, the increase in the electron density with the absorbed power is not linear. Because multistep ionizations become important with the pressure, the decrease in the electron temperature and increase in the electron density become apparent at high pressure. Experimental results agree very well with calculated ones in the wide range of pressure and absorbed power.

[1] M. A. Lieberman, V. A. Godyak, IEEE Trans. Plasma Sci. **26**, 955 (1998).
[2] M. A. Lieberman and A. J. Lichtenberg, *Principles of Plasma Discharges and Materials Processing*, 2nd ed. (Wiley, New York, 2004).
[3] J. Hopwood, C. R. Guarnieri, S. J. Whitehair, and J. J. Cuomo, J. Vac. Sci. Technol. A **11**, 152 (1993).
[4] M. S. Barnes, J. C. Forster, and J. H. Keller, Appl. Phys. Lett. **62**, 2622 (1993).
[5] J. Hopwood, Appl. Phys. Lett. **62**, 940 (1993).
[6] J. A. O'Neil, M. S. Barnes, and J. H. Keller, J. Appl. Phys. **73**, 1621 (1993).
[7] J. Hopwood, Plasma Sources Sci. Technol. **1**, 109 (1992).
[8] V. A. Godyak, R. B. Piejak, and B. M. Alexandrovich, Plasma Sources Sci. Technol. **11**, 525 (2002).
[9] Dimitris P. Lymberopoulos and Demetre J. Economou, J. Appl. Phys. **73**, 3668 (1993).
[10] G. A. Hebner, J. Appl. Phys. **80**, 3215 (1996).
[11] M. Tadokoro, H. Hirata, N. Nakano, Z. Lj. Petrovic, and T. Makabe, Phys. Rev. E **58**, 7823 (1998).
[12] A. Okigawa, M. Tadokoro, A. Itoh, N. Nakano, Z. Lj. Petrovic, and T. Makabe, Jpn. J. Appl. Phys., Part 1 **36**, 4605 (1997).
[13] T. Sato and T. Makabe, J. Appl. Phys. **97**, 113304 (2005).
[14] F. Tochikubo, Z. Lj. Petrovic, N. Nakano, and T. Makabe, Jpn. J. Appl. Phys., Part 1 **33**, 4271 (1994).
[15] M. H. Lee and C. W. Chung, Phys. Plasmas **12**, 73501 (2005).
[16] M. H. Lee and C. W. Chung, Appl. Phys. Lett. **87**, 131502 (2005).
[17] V. A. Godyak, R. B. Piejak, and B. M. Alexandrovich, Plasma Sources Sci. Technol. **1**, 36 (1992).
[18] C. W. Chung, S. S. Kim, and H. Y. Chang, Phys. Rev. E **69**, 016406 (2004).
[19] J. I. Fernandez Palop, J. Ballesteros, V. Colomer, and M. A. Hernandez, Rev. Sci. Instrum. **66**, 4625 (1995).
[20] J. Hopwood, Plasma Sources Sci. Technol. **3**, 460 (1994).
[21] W. F. Edigell, *Argon, Helium and the Rare Gases* (Interscience, New York, 1961), p. 132.
[22] Sumio Ashida, C. Lee, and M. A. Lieberman, J. Vac. Sci. Technol. A **13**, 2498 (1995).
[23] F. Kannari, M. Obaraa, and T. Fujioka, J. Appl. Phys. **57**, 4309 (1985).
[24] N. L. Bassett and D. J. Economou, J. Appl. Phys. **75**, 1931 (1993).
[25] David R. Lide, *CRC Handbook of Chemistry and Physics*, 80th ed. (CRC Press, Boca Raton, 2000).
[26] N. Sadeghi-Kharrazi, thesis, Grenobel, 1974 (unpublished).
[27] V. A. Godyak, *Soviet Radio Frequency Discharge Research* (Delphic Associates, Falls Church, 1986).
[28] K. Suzuki, K. Nakamura, H. Ohkubi, and H. Sugai, Plasma Sources Sci. Technol. **7**, 13 (1998).
[29] U. Kortshagen, N. D. Gibson, and J. E. Lawler, J. Phys. D **29**, 1224 (1996).
[30] Y. Miyoshi, Z. Lj. Petrovic, and T. Makabe, J. Phys. D **35**, 454 (2002).
[31] V. A. Godyak and R. B. Piejak, Phys. Rev. Lett. **65**, 996 (1990).
[32] C. W. Chung and H. Y. Chang, Appl. Phys. Lett. **80**, 1725 (2002).